2021

Parametric Studies On A New Schukey Type Rotary Compressor

Bin Cui
Hochschule Hannover, bin.cui@hs-hannover.de

Martin Gottschlich
Hochschule Hannover

Ulrich Lüdersen
Hochschule Hannover

Stephan Kabelac
Gottfried Wilhelm Leibniz Universität Hannover

Parametric Studies On A New Schukey Type Rotary Compressor

Bin CUI[1*], Martin GOTTSCHLICH[1], Ulrich LÜDERSEN[1], Stephan KABELAC[2]

[1]Hochschule Hannover, Institute for Process & Energy Engineering and Climate Protection, Hannover, Germany
Phone: +49 (0)511-9296-1652, E-Mail: bin.cui@hs-hannover.de, martin.gottschlich@hs-hannover.de, ulrich.luedersen@hs-hannover.de

[2]Gottfried Wilhelm Leibniz Universität Hannover, Institute for Thermodynamics, Hannover, Germany
Phone: +49 (0)511-762-2277, E-Mail: kabelac@ift.uni-hannover.de

*Corresponding Author

ABSTRACT

Efficient compressors are generally important for applications in air conditioning and refrigeration systems. Therefore, innovative technologies are needed to improve their performance and expand their area of application. A new type of rotary compressor, called “Schukey compressor”, has been investigated both experimentally and theoretically. The Schukey-technology goes back to its founder Jürgen Schukey in 1987, who invented a special gear that enables two rotors to rotate out of phase in the same direction within the compressor housing. Each rotor consists of four rectangular shaped piston wings that interlock and perform non-uniform rotary movements, leading to a periodic change of the working chamber volume. During one revolution of the main shaft, 32 compression cycles are performed. Except for our own research work, no further development on this new device is known to us.

Initial studies have shown that changes in the geometrical design of the machine, especially the position of the suction and discharge ports, have a direct influence on thermodynamical variables e.g. technical work, mass flow or pressure ratio. In this contribution, a parametric study is presented to determine the performance of the machine and to show optimization potentials with regard to the volumetric efficiency. The impact of the annular gap and port size variations is examined by using numerical CFD analysis. It is shown that the annular gap size does has a big impact on the mass flow rate and volumetric efficiency. In order to maintain a high efficiency, the gap size should be kept at least below 0.1 mm, where an efficiency of 85.3% is given. An enlargement of the discharge ports leads to an improvement of the volumetric efficiency up from 85.3% to almost 92% but also leads to a decrease of the pressure ratio at the same time since the compression phase ends off earlier. An enlargement of the inlet ports shows no significant effect in terms of pressure ratio and volumetric efficiency. By using the determined surface plots, the size of the ports can be estimated and adjusted according to the intended application of the compressor.

1. INTRODUCTION

In the past, several types of positive displacement rotary compressors have been used in various applications e.g. air conditioning, refrigeration systems and air-compression. These cover lobe-type, screw-type, vane-type and liquid ring-type machines which work with one or more rotating components that either interlock like screws and lobes or pressure the fluid against the chamber walls. The complex components of screw- and rolling piston-type compressors require costly maintenance and manufacture. Unlike reciprocating compressors, rotary compressors in general do not use valves to control the in- and outflow of the gas.

A new rotary type compressor called “Schukey compressor” was first invented and named after its inventor Jürgen Schukey (Schukey, 1987). He originally designed the machine to be operated as a compression or expansion machine for refrigeration applications. Since then, the interest of the machine was fading. Further research on the machine was only done by Meyer (2019), who experimentally determined the heat transfer coefficient within a working chamber when the machine was operated as an expansion machine in a Rankine power cycle. Except for our own research, no investigations as a compressor have yet been carried out.

Numerical methods as well as the increasing computational power became more and more relevant for the development of compressors. A very important tool over the last years is computational fluid dynamics (CFD), where a lot of research work was done in the past. Shiva Prasad (2004) discussed the benefits and risks for using CFD in the development process of positive displacement compressors. Besides, Fagotti and Possamai (2000) have shown the difficulties of using CFD in the compressor design process, where success highly depends on proper boundary conditions, fine meshing, high computing time and choosing the right modelling approaches. Rodrigues (2014), Rovaris and Deschamps (2006) have investigated several approaches for turbulence modelling in reciprocating compressors considering large-eddy simulations (LES) and RANS-equations, finding out that turbulence modelling is just slightly dependent for the accuracy compared to experimental data. Moreover, Farzaneh-Gord et al. (2015) investigated real and ideal gas models for reciprocating compressors, showing that differences in indicated work and mass flow rates do exist. In addition, Branch (2014) compared two real gas equation-methods with the ideal gas equation in a scroll compressor, determining deviations of mass flow rates and an energy efficiency ratio (EER) up to 14%. Due to the high computational effort of CFD-simulations, other numerical approaches like 0D- or 1D-models have been developed in the past and are still used today, mostly on the basis of the 1st law of thermodynamics to model fluid and heat transfer flows for reciprocating compressors (Tuhovcak et al., 2015). Moreover, the coupling of 0D/1D- with 3D-tools was done by Lang et al. (2008) to simulate the suction line of a hermetic reciprocating compressor.

However, most of the work above only consider the simulation of reciprocating compressors. For rotary compressors, such approaches are rare. Especially for the Schukey compressor no numerical calculations were done yet. In this paper, the design, working principle and possible advantages of the Schukey compressor are discussed and presented.

2. DESIGN AND WORKING PRINCIPLE OF THE MACHINE

2.1 Design of the Schukey compressor

The main components of the examined machine are two interlocking rotors with four wings each, that create eight moving chambers within the housing. The rotational movement of each rotor is specified through its own gearbox with special toothed gears. This allows the change of rotational speeds relative to each other known as the characteristic oscillating “Schukey movement” of the compressor. Both rotors rotate in the same direction, with one rotor accelerating and the other rotor retarding vice versa while the main shaft rotates constantly. As a result, the chambers fluctuate in volume, which lead to its suction, compression and discharge movement. Since the compressor is working without suction and discharge valves, the suction, compression and discharge phases are controlled depending on the position of the inlet and outlet ports. A total of 32 compression cycles are performed during one revolution, which leads to a high-volume turnover of the machine. Compared to screw- and rolling piston-type compressors, possible advantages of the Schukey compressor are fast maintenance and low-cost potential due to the simple construction of the rectangular piston wing geometry. Figure 1 is showing the main components of the Schukey compressor in an exploded view.

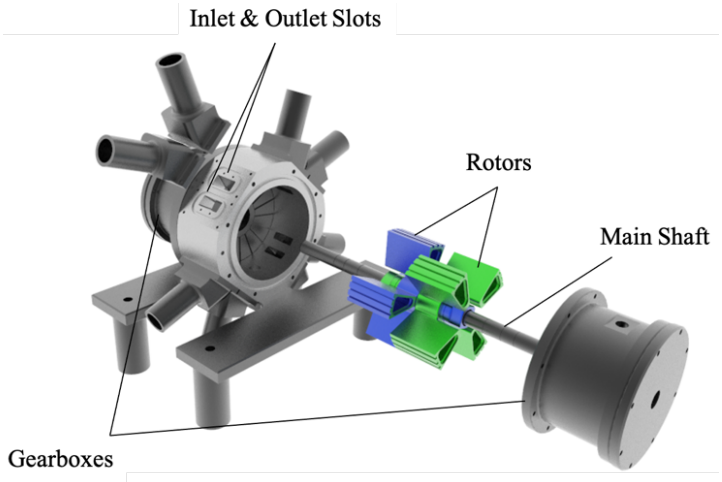

Figure 1: Exploded view of the Schukey compressor.

2.2 Compression cycle

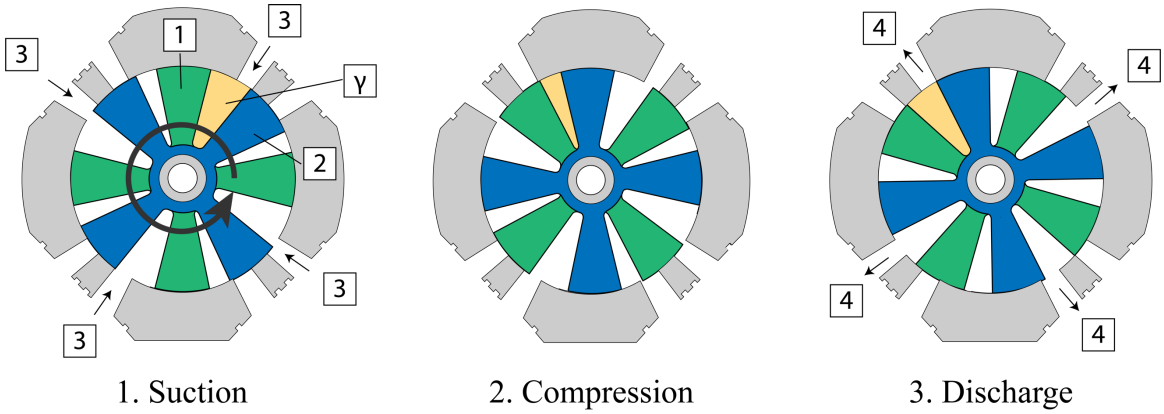

Figure 2: Compression cycle, Rotor 1 (green), Rotor 2 (blue), Chamber (yellow).

In Figure 2 the compression cycle is shown in three steps. Each cycle begins with the filling of the fluid into the working chamber γ through the inlet port (3). During the suction process, the leading rotor (1) is in its accelerating phase of its movement pattern while the complementary rotor (2) is retarding. In that case, the working chamber increases in volume and the fluid is sucked in. This step ends, when rotor blade (2) closes the inlet port during the counter-clockwise rotation. In that moment, the chamber volume is at its maximum. After closing the inlet, rotor blade (2) starts accelerating while rotor blade (1) starts retarding and thus the chamber volume begins to decrease. Since the working chamber is not connected to any inlet- or outlet port, the compression takes place between rotor blade (1) and (2). After reaching its minimum volume, rotor blade (1) passes the outlet port (4) and the fluid will be discharged. From then on, rotor blade (1) starts to accelerate while rotor blade (2) starts to retard again. The discharge process ends when rotor blade (2) passes and closes the outlet port. From then on, the compression cycle starts again.

The cycle takes places in all chambers simultaneously. Therefore, one revolution of the main shaft leads to 32 compression cycles (8 chambers x 4 sections). The compressor is working without active valves and thus does not need any active control mechanism. The oscillating specific movement pattern for each rotor is determined by its own special toothed gears, which are installed with an offset of 45° to each other and connected to the main shaft.

2.3 Kinematics of the Schukey Compressor

The main shaft rotates at a constant speed, driven by an electric motor. As mentioned, the angular velocities of the rotors are not constant, but oscillating and rotating faster or slower than the main shaft. This results in an accelerating and retarding movement. The relative changes in angular velocity of the rotors are shown in Figure 3, where each rotor passes four minima and four maxima during one revolution of 360° of the main shaft. At the moment, when maxima and minima occur, the chamber angle is in its neutral position of 21°. If the angular velocity curves intersect, the chamber volume reaches its minima or maxima, depending on which chamber is actually considered. This is when the compression or the suction ends.

The angular velocity function of each rotor is determined through incremental measurements of the resulting motion of the gearbox. A non-linear regression with the Levenberg-Marquardt-Algorithm was used to determine the coefficients a, b, c and d of eq. (1) and (2). ω_θ is the (constant) angular velocity of the main shaft. With θ as the crank angle, ω_N being the nominal angular velocity and k_b as an additional constant, the angular velocity of each rotor can be calculated with eq. (1) and (2). The resulting chamber angle- and volume function $\gamma(t)$ and $V_C(\gamma)$ can be derived from the angular velocities in eq. (3) and (4), showing a sine-like behavior illustrated in Figure 3. The geometrical dimensions are represented in Table 2.

Angular Velocity Function:

$$\omega_{R1}(\theta) = \left\{-a \cdot \left[1 - cos\left(\frac{\pi}{45°} \cdot \theta + b\right) + \frac{c}{2} \cdot sin^2\left(\frac{\pi}{45°} \cdot \theta + b\right)\right] + d\right\} \cdot k_b \cdot \frac{\omega_\theta}{\omega_N} + \omega_\theta \quad (1)$$

$$\omega_{R2}(\theta) = \left\{-a \cdot \left[1 - cos\left(\frac{\pi}{45°} \cdot \theta + b + \pi\right) + \frac{c}{2} \cdot sin^2\left(\frac{\pi}{45°} \cdot \theta + b + \pi\right)\right] + d\right\} \cdot k_b \cdot \frac{\omega_\theta}{\omega_N} + \omega_\theta \quad (2)$$

Table 1: Determined coefficients of the angular velocity function

Coefficients	a	b	c	d
Values	0.09316	6.28992	0.77746	0.11127

Chamber Angle Function

$$\gamma(t) = \gamma(t - dt) + \int \omega_{R1,2} - \omega_{R2,1}\, dt \tag{3}$$

Volume Chamber Function

$$V_C(\gamma) = l \cdot \frac{\pi}{360°} \cdot \gamma \cdot \left(R_a^2 - R_i^2\right) \tag{4}$$

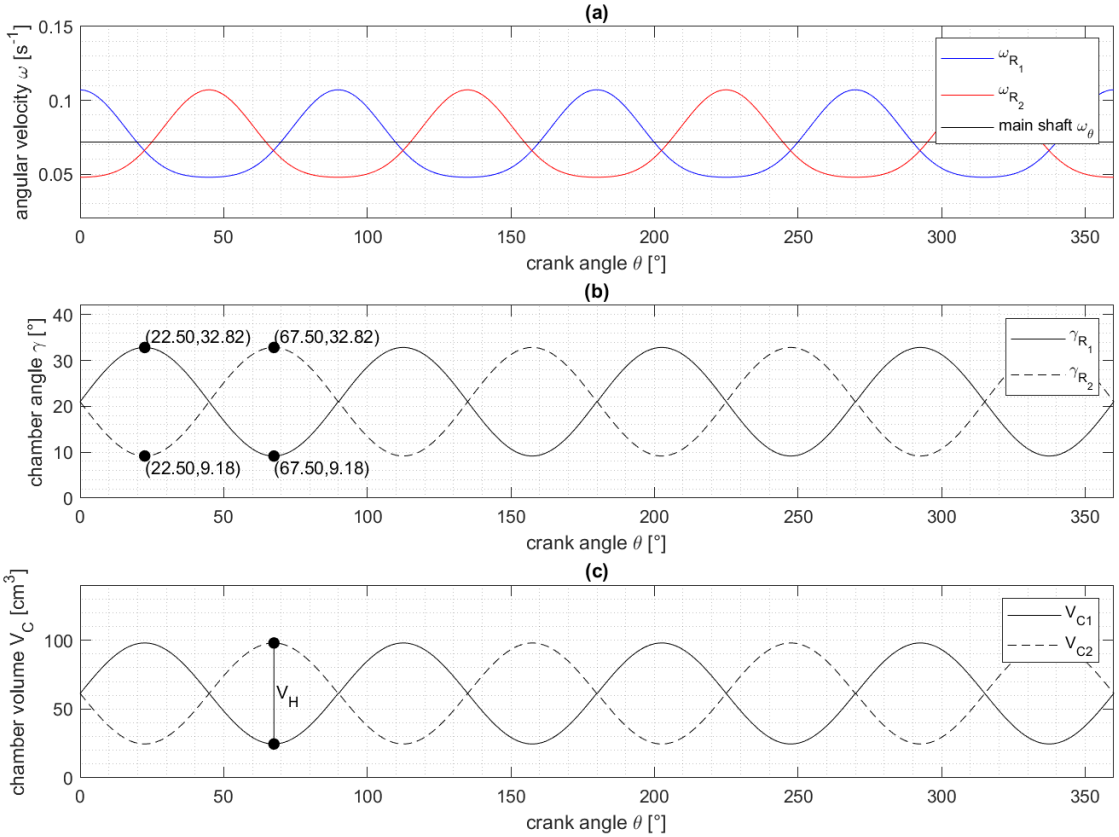

Figure 3: Function of **(a)** angular velocity ω of rotors and main shaft at $\omega_0 = \omega_N = 0.717\ s^{-1}$ =const., **(b)** chamber angle γ with $\gamma_{max} = 32.82\ °$ and $\gamma_{min} = 9.18\ °$, **(c)** chamber volume V_C during one revolution of the main shaft.

Table 2: Compressor geometry parameters.

Compression Chamber			
Min. chamber angle γ_{min}	9.18°	Max. chamber angle γ_{max}	32.82°
Min. chamber volume V_{min}	28.46 cm³	Max. chamber volume V_{max}	101.82 cm³
Stroke volume V_H	73.36 cm³	Total volume turnover per revolution	2.35 l
Rotor dimensions		Suction and discharge Ports	
Outer rotor radius R_a	75 mm	Suction port	8°
Inner rotor radius R_i	22.75 mm	Discharge port	4°
Rotor length l	69.6 mm		
Rotor blade angle	24.0°		

3. SIMULATION MODEL AND STUDY DESIGN

3.1 Preliminary investigations from experimental measurements

The preliminary experimental investigations from the testing facility of Meyer (2019) provide a basis for the simulation model. The mass flow rate has been measured in the testing facility at a rotational speed of 100 rev/min, showing an average mass flow rate of $\dot{m} = 100 \frac{kg}{h}$ (see Figure 4). Further experimental investigations on a new Schukey prototype will be carried out in the near future.

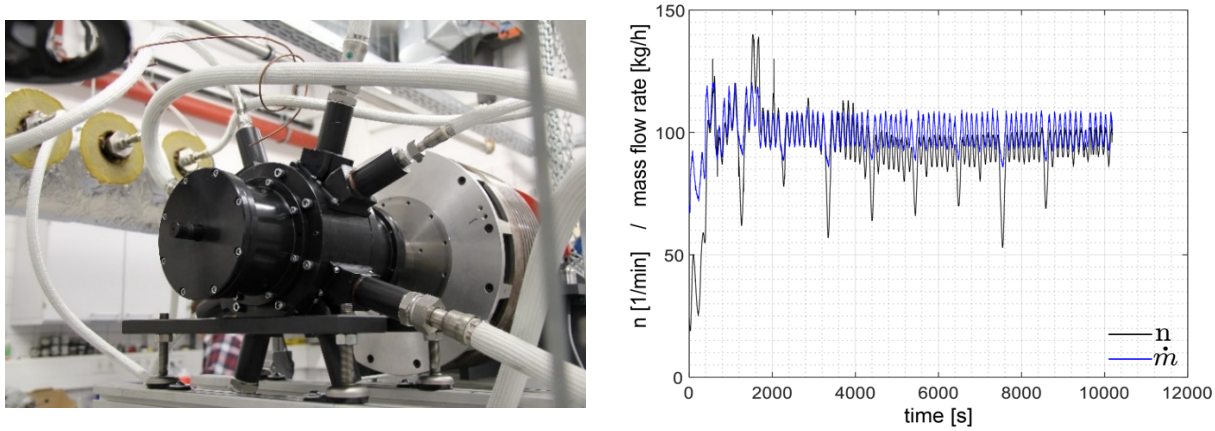

(a) **(b)**

Figure 4: Experimental mass flow rate measurements by Meyer (2019). **(a)** Machine in its testing facility, **(b)** Measurement of mass flow rate and rotational speed of 100 rev/min.

3.2 Equations of State

A very simple model used in CFD-simulations is the ideal gas model, which represents an idealized state neglecting all intermolecular interactions. The results are sufficient accurate as long as the pressure level is low and the occurring temperatures are high. However, in processes with higher densities like in compression cycles or with gaseous states close to its dew line, the model can lead to significant deviations in fluid flow behavior. In order to obtain the most accurate results, real gas equation-models are required. One method to integrate real gas equations in the used CFD-solver ANSYS CFX is the implementation of the NIST Refprop database (Version 9) with RGP-Tables, which contains access to the real gas properties of the chosen fluid. Another approach is the use of real gas models like the Aungier-Redlich-Kwong (ARK) equation of state. In section 4, the ideal and real gas models are compared to each other in a pressure-volume diagram.

3.3 Model

In order to solve the fluid flow of the refrigerant through the compressor, the commercial CFD solver ANSYS CFX Version 2020 R2, based on finite volume method has been used.

One method to simulate the chamber volumes in positive displacement machines is the immersed boundary method (IBM), first introduced by Peskin (2002). Since then, several efforts have been made to enhance the range of applicability and accuracy (Ghias et al., 2007; Kang et al., 2009). For this method, a background mesh and a mesh for the solid rotor body is required. At the overlaps of both meshes, momentum sources are applied to the fluid, representing the rotor movement. Since there are several restrictions for the IBM among other things its usage only for single-phase incompressible fluids, this method is not eligible to model the compressibility effects inside the Schukey compressor. Another way to model the fluctuating volumes of the chambers is the use of remeshing methods, where a new mesh is generated once the deformed mesh is of poor quality. However, each remeshing iteration leads to high computational time. Therefore, a moving mesh model has been used for the hexa-meshed working chambers. For those, a given mesh stiffness was defined which enables the mesh to be deformed but still maintain a high quality. During the compression cycles, the orthogonal angle criteria >80° is still met and varies between 84° and 90°.

In order to keep the computational effort low, the developed simulation model has been split into rotor- and stator domains with different element types, connected through a GGI (Generalized grid interface) that consider the conversation of timestep dependent connection of the fluxes (see Figure 5). The inlet, outlet and annular gap are defined as the stator domain, while rotor 1 and 2 are defined as rotor domains. The rotors are rotating in counterclockwise direction with fluctuating volumes. Since the design of the machine is symmetrical, periodic boundary conditions are set to take the fluid behavior from neighboring domains into account. Therefore, only ¼ of the whole engine was modelled to save computational time. In total, the mesh contains 11,238,409 nodes and 13,121,510 elements.

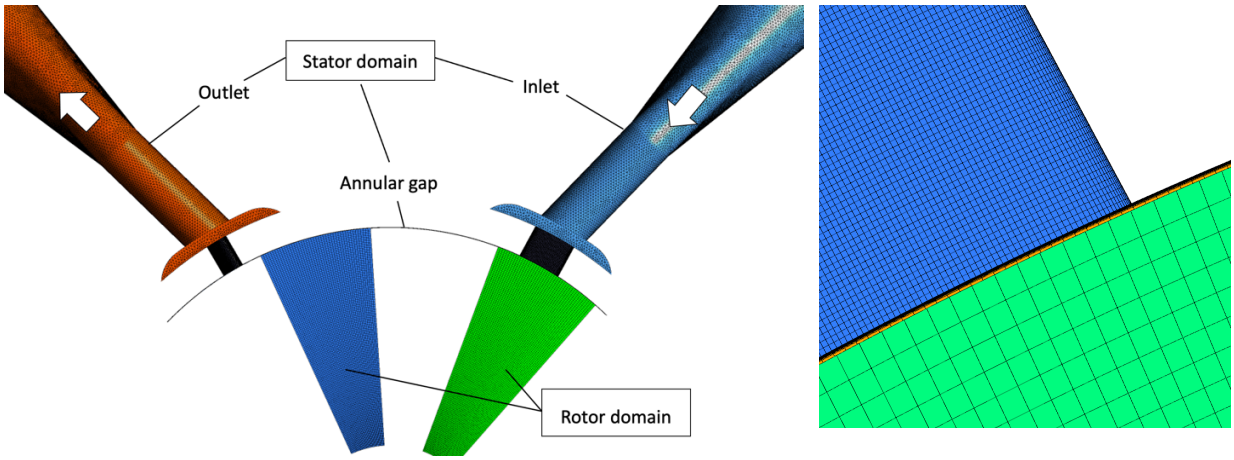

Figure 5: Simulation model**, (a)** Rotor and stator domains**, (b)** Mesh grid interfaces.

3.4 Boundary conditions

In order to simulate reliable numerical results, a highly fine meshed model and an adequate setup of boundary conditions are required. In this work, different boundary conditions are assumed. Some remain constant during all calculations according to Table 3 and some vary for the parametric study, listed in Table 4. The pressure and temperature at inlet and outlet are specified as opening conditions that enable fluid flows in both directions in and out of the domain. Both, inlet and outlet pressure remain constant. The rotational speed of the main shaft is set constant with 1200 rpm since it has shown very good results in initial studies. To describe the characteristic movement of the rotor wings, specified displacement functions of the left and right rotor walls are set in CFX Expression Language (CEL). Since there were only preliminary measurements of the heat transfer coefficient by Meyer (2019), it is assumed to be constant on the outer walls with 150 W/m²K with an ambient temperature of 35 °C. For turbulence modelling, the Reynolds Averaged Navier Stokes Equations (RANS) are chosen, which solve the average flow behavior separately from unsteady contributions. The Shear Stress Transport (SST) model from Menter (1994) is used since it combines the advantages of the k-ε and the k-ω model and has proven to be suitable for most engineering flows, providing good results and a robust scheme. The simulation considers two full revolutions, in total eight full compression cycles for each chamber, to obtain enough time for flow development inside the machine.

3.5 Parametric study design

Since the machine is operating without active valve mechanisms, a good sealing of the working chambers needs to be ensured. The resulting leakage flow out of the working chamber is modelled by the circumferential annular gap, which varies between 0 mm and 0.2 mm for the parametric study in order to examine the impact of leakage regarding mass flow rate, pressure ratio and volumetric efficiency.

Furthermore, past investigations have shown that the size of the suction and discharge ports can also have a big impact on the mentioned values. Therefore, the correlation between the size of the ports in terms of volumetric efficiency and pressure ratio is determined without permitting a parasitic flow as a result of the direct connection of both openings. The annular gap size in this case was kept constant with 0.1 mm.

It is also of interest to estimate the difference between the ideal gas and real gas models, since the computing time of real gas models is considerably longer. Because of that, the results from the ideal gas-, ARK- and RGP-model are compared to each other in a pressure-volume diagram.

Table 3: Boundary conditions used in simulation.

Boundary condition	Value
Suction pressure	1 bar
Discharge pressure	1.8 bar
Inlet temperature	300 K
Wall heat transfer coeff.	150 W/m²K
Outside temperature	308 K
Rotational speed main shaft	1200 rpm

Table 4: Parametric values.

Parametric variables	Values
Fluid	Air ideal gas, Air ARK-model, Air RGP-Table
Annular gap	0 mm – 0.2 mm
Suction port size	8-16°
Discharge port size	4-14°

4. SIMULATION RESULTS

To compare the results of the parametric studies, pressure-volume diagrams and 3-dimensional surface plots have been created and are shown in Figure 6 and Table 5. Since there is no experimental data available, only simulation results are compared to each other.

The pressure-volume diagram in Figure 6 (a) presents the comparison between the ideal gas-, ARK- and RGP model. The graph only shows small deviations between the compared models, which can also be seen at the results in Table 5. The volumetric efficiency merely deviates about $\pm$ 1% and the internal pressure ratio only differs by $\pm$ 0.03. Therefore, the impact of using real gas models over the ideal gas model is small at these pressure levels and can be neglected to save computational effort.

Figure 6 (b) shows the results of the annular gap study, which do have a more significant impact on the performance, especially at higher pressure areas in this machine. Comparing the gap sizes 0 mm and 0.2 mm, the internal pressure ratio decreases by 0.3 due to the leakage of the fluid. The leakage also leads to a decreased mass flow rate of the machine, which on the other hand, results in a decreasing volumetric efficiency as seen in Table 5 and Figure 6 (c). Without considering an annular gap at all, the volumetric efficiency is nearly ideal with 99.7%. With a growing gap size, the efficiency starts to decrease slowly until a gap size of 0.05 mm with a volumetric efficiency of 97.8% is reached. From then on, the efficiency drops significantly to 85,3% at a gap size of 0.1 mm and 68.5% at the gap size of 0.15 mm. At 0.2 mm the mass flow rate is lowered by nearly 50% which should be avoided for the upcoming prototype of this machine. In order to maintain a high volumetric efficiency >85%, the annular gap size should be kept at least below 0.1 mm, which can be feasible with high manufacturing quality and a good sealing concept.

Lastly, the results of the parametric study on different suction and discharge port sizes are shown in Figure 6 (d-f). The mass flow rate (d) shows an analogous behavior to the volumetric efficiency (e), where a growing suction port size results in no significant improvement of the volumetric efficiency nor the internal pressure ratio. An enlargement of the discharge ports, however, leads to an increase of the volumetric efficiency up to 92% but comes, on the other hand, with a reduction of the internal pressure ratio from its maximum 2.73 to 1.95. This behavior is to be expected and can be explained by the fact, that when the discharge port size is enlarged, the compression phase breaks off earlier and a relatively longer ejection process takes place. The chamber volume has not reached its small volume yet to build up a high pressure. Therefore, it should be prioritized whether a higher pressure ratio or a higher volumetric efficiency is more important. For the intended application, the optimal size of the ports can then be estimated based on the determined surface plots.

Table 5: Results of the parametric studies for real- and ideal gas comparison and annular gap size.

Variable	Internal pressure ratio	MFR	Volumetric Efficiency
	Π	$\dot{m}$	λ
Unit	–	kg/s	%
Air ideal	2.82	0.0506	89.4
Air ARK	2.79	0.0513	90.6
Air RGP	2.84	0.0503	88.8
0 mm	2.81	0.0563	99.7
0.05 mm	2.78	0.0544	97.8
0.1mm	2.73	0.0473	85.3
0.15 mm	2.65	0.0379	68.5
0.2 mm	2.55	0.0274	49.6

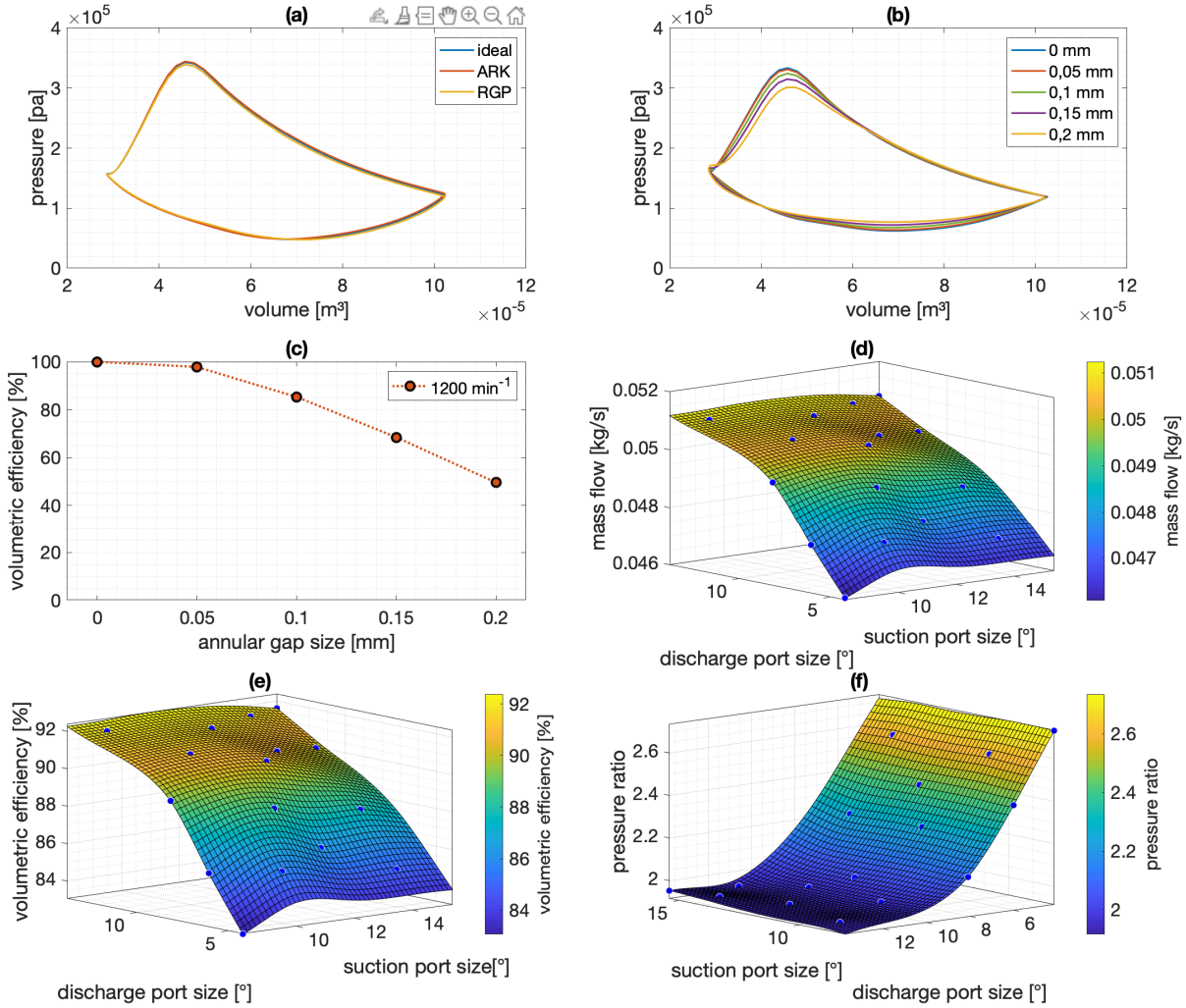

Figure 6: Results of parametric studies at 1200 rev/min: **(a)** Pressure-volume diagram for air ideal gas-, ARK- and RGP model, **(b)** Pressure-volume diagram for annular gap size variation, **(c)** Volumetric efficiency for annular gap size variation, **(d)** Mass flow rates for suction/discharge port size variation, **(e)** Volumetric efficiency for suction/discharge port size variation, **(f)** Internal pressure ratio for suction/discharge port size variation.

5. CONCLUSIONS

A new rotary type compressor named Schukey compressor has been introduced. The working principle is based on two phase-shifted rotors, which are realized by special toothed gears. The construction and working principle are relatively easy due to the simple shape of the rectangular piston wings. Compared to other rotary compressors, this new compressor has a great potential for the application in refrigeration systems because of its high volume turnover. Due to the operation without oil and active valves systems, the compressor requires low maintenance making it more sustainable for the environment after all.

It was shown that the annular gap size does have a high impact regarding mass flow rate and volumetric efficiency. In order to maintain a high efficiency, the gap size should be kept below 0.1 mm, where an efficiency of 85.3% is given. At a gap size of 0.05 mm, the efficiency increases to 97.8% which should be aimed for in the manufacturing process and its sealing concept. Furthermore, this paper showed the differences between using ideal gas and real gas equations. The examined real gas models ARK and RGP only showed small deviations by ± 1% in volumetric efficiency compared to the ideal gas model and therefore can be neglected for the existing pressure range. Lastly, the relation between different suction and discharge port sizes were examined, where an enlargement of the suction port size led to no significant difference in internal pressure ratio and volumetric efficiency. In spite of that, an enlargement of the discharge port size has led to a higher volumetric efficiency from 85.3% to nearly 92%, but comes, on the other hand, with a lower pressure ratio since the compression phase breaks off earlier. Depending on the application, it should be prioritized whether a higher pressure ratio or a higher volumetric efficiency is needed. By using the determined surface plots, the size of the ports can then be estimated and adapted accordingly to its use case.

The machine, however, is still in its development phase where further optimization possibilities exist like finding the optimal wing geometry or changing the kinematic function of the gear. Further investigations are concentrated on these points. Even though the results show high potential in use for air refrigeration processes, the methodology still requires to be fully validated with experimental data before extending analyses should be done.

NOMENCLATURE

ARK	Aungier-Redlich-Kwong	(–)
CFD	Computational Fluid Dynamics	(–)
CEL	CFX Expression Language	(–)
EER	Energy-efficiency-ratio	(–)
EOS	Equation of State	(–)
FSI	Fluid-Structure Interaction	(–)
GGI	Generalized grid interface	(–)
IBM	Immersed boundary method	(–)
LES	Large Eddy Simulation	(–)
MFR	Mass flow rate	$(kg \cdot s^{-1})$
NIST	National Institute of Standards and Technology	(–)
RANS	Reynolds Averaged Navier Stokes	(–)
RGP	Real gas properties	(–)
SST	Shear Stress Transport	(–)
λ	Volumetric Efficiency	(%)
ω	Angular velocity	(s^{-1})
θ	Crank angle	(°)
γ	Chamber angle	(°)
Π	Internal pressure ratio	(–)

Subscript

1,2	Rotor number
θ	Main shaft
c	Chamber
N	nominal

6. ACKNOWLEDGEMENT

This work was supported by the compute cluster, which is funded by the Leibniz Universität Hannover, the Lower Saxony Ministry of Science and Culture (MWK) and the German Research Association (DFG).

7. REFERENCES

Branch, S. (2014). Methods of fluid properties for compressible refrigerant CFD analysis. In International Compressor Engineering Conference (Ed.), *22nd International Compressor Engineering Conference at Purdue 2014: West Lafayette, Indiana, USA, 14-17 July 2014* (pp. 155–165). Curran Associates Inc. https://docs.lib.purdue.edu/icec/2289/

Fagotti, F., & Possamai, F.C. (2000). Using Computational Fluid Dynamics as a Compressor Design Tool: Paper 1377. In International Compressor Engineering Conference (Chair), *International Compressor Engineering Conference,* Purdue.

Farzaneh-Gord, M., Niazmand, A., Deymi-Dashtebayaz, M., & Rahbari, H. R. (2015). Thermodynamic analysis of natural gas reciprocating compressors based on real and ideal gas models. *International Journal of Refrigeration*, *56*, 186–197. https://doi.org/10.1016/j.ijrefrig.2014.11.008

Ghias, R., Mittal, R., & Dong, H. (2007). A sharp interface immersed boundary method for compressible viscous flows. *Journal of Computational Physics*, *225*(1), 528–553. https://doi.org/10.1016/j.jcp.2006.12.007

Kang, S., Iaccarino, G., & Ham, F. (2009). DNS of buoyancy-dominated turbulent flows on a bluff body using the immersed boundary method. *Journal of Computational Physics*, *228*(9), 3189–3208. https://doi.org/10.1016/j.jcp.2008.12.037

Lang, W., Almbauer, R., Burgstaller, A., & Nagy, D. (2008). Coupling of 0-,1- and 3-d Tool for the Simulation of the Suction Line of a Hermetic Reciprocating Compressor: Paper 1881. In International Compressor Engineering Conference (Chair), *International Compressor Engineering Conference 2008,* Purdue.

Menter, F. R. (1994). Two-equation eddy-viscosity turbulence models for engineering applications. *AIAA Journal*, *32*(8), 1598–1605. https://doi.org/10.2514/3.12149

Meyer, J. (2019). *Experimentelle Bestimmung und Modellierung des Wandwärmeübergangs innerhalb eines Drehkammerschwingsystems* [Dissertation]. Gottfried Wilhelm Leibniz Universität, Hannover.

Peskin, C. S. (2002). The immersed boundary method. *Acta Numerica*, *11*, 479–517. https://doi.org/10.1017/S0962492902000077

Rodrigues, T. T. (2014). Tubulence Modelling Evaluation for Reciprocating Compressor Simulation: Paper 2297. In International Compressor Engineering Conference (Ed.), *22nd International Compressor Engineering Conference at Purdue 2014: West Lafayette, Indiana, USA, 14-17 July 2014.* Curran Associates Inc.

Rovaris, J. B., & Deschamps, C. J. (2006). Large eddy simulation applied to reciprocating compressors. *Journal of the Brazilian Society of Mechanical Sciences and Engineering*, *28*(2), 208–215. https://doi.org/10.1590/S1678-58782006000200010

Schukey, J. (1987). European Patent Office : Drehkolbenmaschine(0316346). Germany.

Shiva Prasad, B. G. (2004). CFD for Positive Displacement Compressors: Paper 1689. In International Compressor Engineering Conference (Chair), *International Compressor Engineering Conference at Purdue,* Purdue. https://docs.lib.purdue.edu/icec/1689

Tuhovcak, J., Hejcik, J., & Jicha, M. (2015). Modelling of fluid flow and heat transfer in a reciprocating compressor. *IOP Conference Series: Materials Science and Engineering*, *90*, 12018. https://doi.org/10.1088/1757-899X/90/1/012018